pISSN 1229-3008 eISSN 2287-6251
Progress in Superconductivity and Cryogenics
Vol.18, No.3, (2016), pp.10~20 http://dx.doi.org/10.9714/psac.2016.18.3.010

Comparisons of internal self-field magnetic flux densities between recent Nb_3Sn fusion magnet CICC cable designs

S. P. Kwon*

National Fusion Research Institute, Daejeon, Korea

(Received 1 August 2016; revised or reviewed 23 September 2016; accepted 24 September 2016)

Abstract

The Cable-In-Conduit-Conductor (CICC) for the ITER tokamak Central Solenoid (CS) has undergone design change since the first prototype conductor sample was tested in 2010. After tests showed that the performance of initial conductor samples degraded rapidly without stabilization, an alternate design with shorter sub-cable twist pitches was tested and discovered to satisfy performance requirements, namely that the minimum current sharing temperature (T_{cs}) remained above a given limit under DC bias. With consistent successful performance of ITER CS conductor CICC samples using the alternate design, an attempt is made here to revisit the internal electromagnetic properties of the CICC cable design to identify any correlation with conductor performance. Results of this study suggest that there may be a simple link between the Nb_3Sn CICC internal self-field and its T_{cs} performance. The study also suggests that an optimization process should exist that can further improve the performance of Nb_3Sn based CICC.

Keywords: fusion magnet, superconducting cable, cable-in-conduit conductor, CICC, cable layout, niobium-tin

1. BACKGROUND

The ITER tokamak jointly being constructed in southern France by 35 countries will be the largest fusion machine ever built to date. ITER will be a fully superconducting tokamak incorporating Nb_3Sn, NbTi and some HTS superconductor technology for its huge magnets and current leads [1].

As a first of a kind machine at industrial scale, many technological innovations have been incorporated in the construction of ITER in order to overcome technical challenges. One of the most widely reported technical challenges has been the problem with the central solenoid (CS) which is a cylindrically shaped superconducting magnet made up of multiple modules that are stacked up vertically to a total height over 13 m and weighing more than 950 tons [2, 3]. The main problem with the magnet was that the Nb_3Sn based Cable-In-Conduit Conductor (CICC) that makes up each module was not performing to requirements during early tests. Specifically, CICC samples subjected to high background field were showing lower and lower current sharing temperature (T_{cs}) without stabilization, with repeated electromagnetic (EM) loading from current cycling [4-7]. The minimum T_{cs} was set at 5.2 K and this requirement was being breached, sometimes after several thousand current cycles, with the original CICC design.

The testing which was performed at the SULTAN facility of the Swiss Plasma Center, located within the Paul Scherrer Institute in Villigen, Switzerland verifies conductor performance under simulated operating conditions within the ITER tokamak [8-10]. The ITER CS CICC which has to operate in magnetic fields up to 12.34 T is expected to be energized 60,000 times over the ITER tokamak lifetime. So, it can be expected that a CS module will eventually fail from CICC performance degradation well before the end of the tokamak working life, requiring costly and time consuming repairs.

The initial design which had not been optimized was adopted after results of simulations and limited testing suggested better overall performance, especially better transverse load support and adequate AC coupling loss, over shorter twist pitch cabling [11, 12]. Premature failure of the design, however, prompted further investigation into improving performance with modified CICC designs. The ITER International Organisation (IO) which is responsible for the design of ITER led a study that uncovered a solution to the problem in the form of a design change to the CICC cable, which brought about a return to shorter sub-cable twist pitches [6, 7, 12, 13]. Additional investigation with different CICC samples confirmed the improved performance from the changed design [6], [13-16]. The new design, referred to as short twist pitch (STP), has since been adopted as the new baseline for ITER CS conductor [17].

2. INTRODUCTION TO ITER CS CONDUCTOR DESIGN AND PERFORMANCE

The cable for the ITER CS CICC is of a complicated

This work was supported in part by the National Fusion Research Institute and the Ministry of Science, ICT and Future Planning of the Republic of Korea under ITER Project Contracts.

* Corresponding author: spkwon@nfri.re.kr

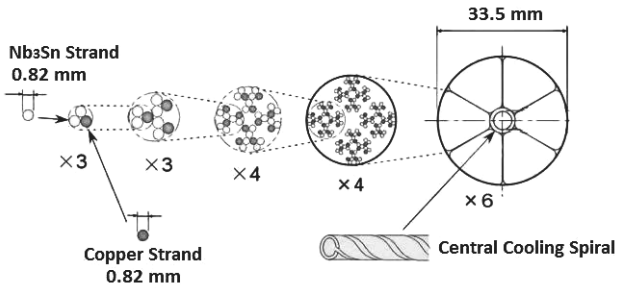

Fig. 1. Cable layout of the ITER CS cable. Light dots represent Nb_3Sn strand whereas dark dots represent Cu strand. A cooling channel exists in the center.

five stage design, as shown in Fig. 1, consisting of 576 Nb_3Sn and 288 Cu strands. Each stage sub-cable has its own twist pitch given in Table I [18, 19]. Dramatic improvement in T_{cs} performance is obtained when the CICC cable design is changed from original to STP design [6, 7, 12-16]. This improvement is regardless of strand design. In other words, it is observed in both Internal-Tin and Bronze type Nb_3Sn strand, in strand that is of slightly thicker or thinner diameter, with strand of different average critical current (I_c), etc. Minor variations in cable parameters have been allowed where they do not seem to affect performance.

The results of the investigation by IO and the subsequent tests on ITER CS CICC samples with STP cable, which are reproduced in Fig. 2, indicate different fundamental behavior between STP and original design cable with EM loading [6]. This strongly suggests that the improvement in conductor performance is not sensitive to minor variation in a cable parameter but an indication of a significant change, kin to a phase transition. The consistent and robust behavior of STP cable CICC, despite the randomness and variation in the construction of each test sample does not suggest otherwise.

The clear characteristics seen in Fig. 2 are the initial improvement followed by stabilization in T_{cs} by CICC samples with STP cable and the gradual T_{cs} degradation by samples with original design cable. The degradation of original design cable has been attributed to many factors: strand breakage, filament fractures within strand, buckling and associated deformation of cable, etc. [4-7, 11-16, 20-28]. In particular, sensitivity of the superconducting properties of Nb_3Sn to strain has been well studied and credited to contribute to performance degradation; the inter-strand contact forces within a cable cause strain with EM loading. Of the identified causes, only strain sensitivity is reversible, and strain relaxation causing an increase in T_{cs} does seem to occur with thermal cycling (WUCD) even in some non-STP CICC samples.

Relaxation in the intrinsic strain of a Nb_3Sn strand sample is currently the only identified mechanism that improves strand I_c, and improvement of I_c leads to improvement of T_{cs} [6, 7, 13, 16, 27]. It follows then that the initial improvement in T_{cs} seen in STP cable CICC is due to the intrinsic strain in the strands being relaxed, initiated by the internal EM forces within the cable. Other factors do contribute. Though not yet quantified, as anyone involved with the production or examination of STP cable can testify, STP cable starting from the very first stage sub-cable is very rigid [13, 16, 29]. Furthermore, there being more material per unit length of conductor due to the shorter twist pitch, the void fraction of STP CICC cable can be expected to be slightly smaller than cable of original design. The combination of these two factors results in CICC cable that is more resistant to deformation. And, sustained performance has been reported in superconducting cable that does not deform under EM loading [30]. However, this does not explain the initial T_{cs} improvement observed in STP cable CICC.

The initial increase in T_{cs} could be explained as a recovery from the intrinsic strain in Nb_3Sn strand due to thermal contraction of the strand from 650 °C when Nb_3Sn is formed during heat treatment to the cryogenic temperatures for superconductivity. Thus, there is a reduction in the maximum strand I_c, which can be

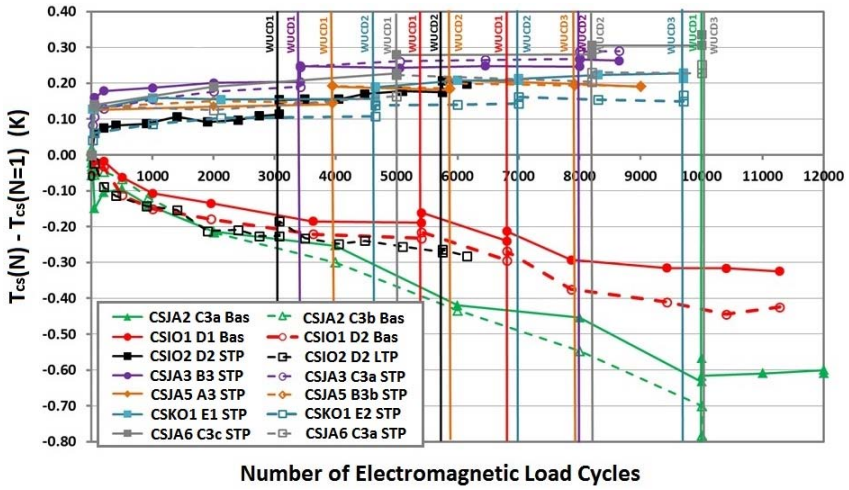

Fig. 2. Plot of the change in T_{cs} with respect to the initial T_{cs} with EM loading for various ITER CS CICC samples identified in the legend. All samples with increasing T_{cs} have STP design cable, and samples with decreasing T_{cs} have original (baseline or Bas) design or long twist pitch (LTP) cable. (Plot courtesy of the ITER International Organisation.)

Table I.
Recently Reported Nb_3Sn based CICC Cable Characteristics and Parameters.

Design Name	ITER TF option 2	ITER TF option 1	CSIO2 right	TFPRO2 OST1	MF HFML STP	ITER CS STP	TFPRO2 OST2	CSIO2 left	MF HFML LTP	CSIO1 right	CSIO1 left	ITER CS original	PITSAM 5S	PITSAM 2	PITSAM 5L
Nominal Current (kA)	68	68	49	68	20	49	68	49	20	49	49	49	17	17	17
Cable Shape	circle	circle	circle	circle	rectangle	circle	circle	circle	rectangle	circle	circle	circle	square	square	square
Cable Layout	ITER TF layout	ITER TF layout	ITER CS layout	ITER TF layout	MF SCH layout	ITER CS layout	ITER TF layout	ITER CS layout	MF SCH layout	ITER CS layout	ITER CS layout	ITER CS layout	PITSAM layout	PITSAM layout	PITSAM layout
No. of SC strands															
1st stage	2	2	2	2	1 or 2	2	2	2	1 or 2	2	3	2	1 or 2	1 or 2	1 or 2
2nd stage	6	6	6	6	6	6	6	6	6	6	9	6	4	4	4
3rd stage	30	30	24	30	24	24	30	24	24	24	36	24	12	12	12
4th stage	150	150	96	150	120	96	150	96	120	96	144	96	48	48	48
5th stage	900	900	576	900		576	900	576		576	864	576			
No. of Cu strands															
1st stage	1	1	1	1	1 or 2	1	1	1	1 or 2	1	0	1	1 or 2	1 or 2	1 or 2
Total	522	522	288	522	120	288	522	288	120	288	0	288	60	60	60
Strand Radius, r_s (mm)	0.410	0.410	0.411	0.405	0.405	0.410	0.405	0.411	0.405	0.410	0.410	0.415	0.405	0.405	0.405
r_i/r_s factors	ITER TF layout	ITER TF layout	ITER CS layout	ITER TF layout	MF SCH layout	ITER CS layout	ITER TF layout	ITER CS layout	MF SCH layout	ITER CS layout	ITER CS layout	ITER CS layout	PITSAM layout	PITSAM layout	PITSAM layout
Twist Pitch, λ_i (mm)															
1st stage	80	45	110	45	20	20	116	22	82	45	45	45	33	58	83
2nd stage	140	85	115	87.5	45	45	182	45	110	83	83	85	95	95	140
3rd stage	190	125	127	126.5	80	80	245	81	135	141	141	145	139	139	192
4th stage	300	250	140	245	160	150	415	159	160	242	252	250	213	213	213
5th stage	420	450	385	460		450	440	443		423	423	450			
Twist Pitch Ratio, β_λ	1.52	1.79	1.50	1.80	2.01	2.23	1.42	2.15	1.25	1.75	1.75	1.78	1.96	1.54	1.39
Strand Current, j_s (A)	75.6	75.6	85.1	75.6	167	85.1	75.6	85.1	167	85.1	56.7	85.1	354	354	354
Void Fraction (%)	29.7		29.1	29.1	26.7		27.7	32.4	26.3	33.4	33.4	33.5	~30	~30	~30

recovered with reverse strain. In order to identify a possible mechanism that gives rise to this reverse strain, correlation between T_{cs} performance and the internal self-field of CICC cable under DC bias, as was the case during testing in SULTAN, was investigated. The differing cabling layouts of the different CICC samples give rise to different internal self-field which in turn should produce different internal EM forces within the cable.

3. SIMPLE MODEL OF CICC CABLE AND ITS MAGNETOSTATIC FIELD

3.1. Basic Principles and First Stage Sub-cable Model

The determination of the internal EM fields inside CICC is very complicated and can involve complex functions or sophisticated numerical tools, even for simplified models of multi-strand multi-stage cable [31-34]. This can be further complicated when attempting to determine the stresses and strain taking into account inter-strand interaction [23, 35-37]. Rather than relying on exact analytical methods or numerical tools, use of the following simple cable model, originally introduced in [38], is used for estimating the field magnitudes. As an example, the simplified model of the internal magnetostatic self-field is described for the ITER CS CICC cable.

First, there are three strands in the first stage sub-cable, each shaped in a helix. With simplification, the sub-cable is modelled as a uniform cable whose current can be decomposed into a circular transverse current around the center of the sub-cable and a longitudinal current along the sub-cable length. See Fig. 3(a). The circular current is then further simplified and modelled as a thin solenoid with uniform magnetic field inside. There is no physical justification for this last step except to say that the field characteristics are similar to zeroth order.

The longitudinal current of the first stage sub-cable can be described as the current in the two superconducting strands multiplied by a correction factor. This is in line with the vast majority of the current flowing in the Nb_3Sn strands and only a little in the Cu strand when in the superconducting state. The nonuniformity in the current is random among all first stage sub-cables. So, the current is taken to be uniform over the cable cross section.

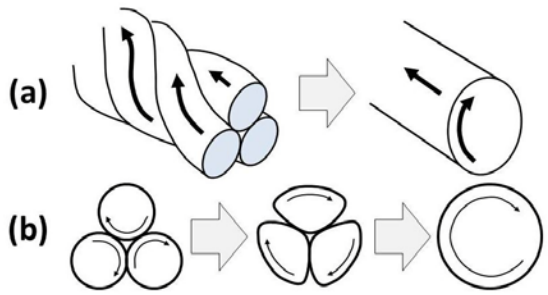

Fig. 3. Simplification of the ITER CS cable. (a) First stage sub-cable is modelled as a uniform longitudinal current over the volume and a uniform circular current over the surface. (b) Simplification of the second stage sub-cable model from three first stage sub-cable models.

To determine the appropriate circular current of the solenoid, we begin with the trajectory of a strand along the z-direction described by the following vector components.

$$x = r_1\, cos(2\pi z/\lambda_1),\ y = r_1\, sin(2\pi z/\lambda_1),\ z \tag{1}$$

where r_1 is the radius of the helix, ideally $2/\sqrt{3}$ times the strand radius for close packing. λ_1 is the twist pitch of the first stage sub-cable. Note that in a length of sub-cable corresponding to λ_1, there are two current carrying strands that complete a full cycle. This ignores the contribution of the Cu strand which only carries small current. Then for a unit length Δz of first stage sub-cable, there are

$$\Delta n = N_1 \Delta z/\lambda_1 \tag{2}$$

turns of circular current where N_1=2. From (1) and (2), the circular transverse current j_1 per unit length Δz in the first stage sub-cable is given by

$$j_1/\Delta z = (j_s N_1/\lambda_1)\cdot(2\pi r_1/\lambda_1)/\sqrt{(2\pi r_1/\lambda_1)^2+1} \tag{3}$$

where j_s is the current in a single strand.

3.2. Second and Subsequent Stage Sub-cable

The second stage sub-cable is the combination of three first stage sub-cables. As seen in Fig. 3(b), there is partial cancellation between the circular transverse currents on the inside of the sub-cable. So, the resulting transverse current of the second stage sub-cable is approximated by a thin solenoidal current, similarly as was done for the first stage sub-cable. The radius of the resulting second stage sub-cable solenoid is approximately $4/3 + 2/\sqrt{3}$ or about 2.5 times the radius of a strand taking into account the outer rim of the thin solenoid and a closely packed triangular configuration.

To this, the twist pitch of the second stage sub-cable adds an additional circular transverse current. In ITER CS conductor, all of the cables and sub-cables have a right-handed twist pitch, so the circular currents are additive. Therefore, ignoring corrections for angular rotation of the axes of the first stage sub-cables, the total circular transverse current j_2 per unit length Δz in a second stage sub-cable is given by

$$j_2/\Delta z = j_s \frac{N_2}{\lambda_2}\frac{2\pi r_2/\lambda_2}{\sqrt{(2\pi r_2/\lambda_2)^2+1}} N_1 + j_s \frac{N_1}{\lambda_1}\frac{2\pi r_1/\lambda_1}{\sqrt{(2\pi r_1/\lambda_1)^2+1}} \tag{4}$$

where N_2=3. The contribution from the second stage sub-cable twist pitch takes into account that there are $N_1 \cdot N_0$ strands for each first stage sub-cable, with N_0=1 being the multiplying factor of the second term on the right-hand-side in (4).

By induction, the total circular transverse current j per unit length Δz for the whole cable is

$$j/\Delta z = \sum_{i=1}^{5} j_s \frac{N_i}{\lambda_i}\frac{2\pi r_i/\lambda_i}{\sqrt{(2\pi r_i/\lambda_i)^2+1}} \prod_{m=0}^{i-1} N_m \tag{5}$$

Table II.
Cable Layouts and r_i/r_s Factors of Recently Reported Nb_3Sn based CICC Cable.

Design Name	ITER TF layout	ITER CS layout	MF SCH layout	PITSAM layout
Cable Layout	((2SC+1Cu)×3×5×5+(3Cu×4))×6	(2SC+1Cu)×3×4×4×6	((2SC+1Cu)×2+(1SC+2Cu)×2)×4×5	((2SC+1Cu)+(1SC+2Cu)×2)×3×4
r_i/r_s factors				
1st stage	$\frac{2}{\sqrt{3}} \approx 1.15$	$\frac{2}{\sqrt{3}} \approx 1.15$	$\frac{2}{\sqrt{3}} \approx 1.15$	$\frac{2}{\sqrt{3}} \approx 1.15$
2nd stage	$\frac{4}{3}+\frac{2}{\sqrt{3}} \approx 2.49$	$\frac{4}{3}+\frac{2}{\sqrt{3}} \approx 2.49$	$\frac{2}{\sqrt{3}}(1+\sqrt{2}) \approx 2.79$	$\frac{4}{3}+\frac{2}{\sqrt{3}} \approx 2.49$
3rd stage	$\left(1+\frac{4}{\sqrt{10-2\sqrt{5}}}\right)\left(\frac{4}{3}+\frac{2}{\sqrt{3}}\right) \approx 6.72$	$(1+\sqrt{2})\left(\frac{4}{3}+\frac{2}{\sqrt{3}}\right) \approx 6.01$	$\frac{2}{\sqrt{3}}(3+2\sqrt{2}) \approx 6.73$	$\left(1+\frac{2}{\sqrt{3}}\right)\left(\frac{4}{3}+\frac{2}{\sqrt{3}}\right) \approx 5.36$
4th stage	$2\left(1+\frac{4}{\sqrt{10-2\sqrt{5}}}\right)\left(\frac{4}{3}+\frac{2}{\sqrt{3}}\right)+(1+\sqrt{2})\left(1+\frac{2}{\sqrt{3}}\right) \approx 18.64$	$(3+2\sqrt{2})\left(\frac{4}{3}+\frac{2}{\sqrt{3}}\right) \approx 14.50$	$\frac{2}{\sqrt{3}}(3+2\sqrt{2})\left(1+\frac{4}{\sqrt{10-2\sqrt{5}}}\right) \approx 18.18$	$(1+\sqrt{2})\left(1+\frac{2}{\sqrt{3}}\right)\left(\frac{4}{3}+\frac{2}{\sqrt{3}}\right) \approx 12.94$
5th stage	$3\left\{2\left(1+\frac{4}{\sqrt{10-2\sqrt{5}}}\right)\left(\frac{4}{3}+\frac{2}{\sqrt{3}}\right)+(1+\sqrt{2})\left(1+\frac{2}{\sqrt{3}}\right)\right\} \approx 55.93$	$3(3+2\sqrt{2})\left(\frac{4}{3}+\frac{2}{\sqrt{3}}\right) \approx 43.50$		

Table III.
Zeroth Order Estimation of Internal Magnetostatic Self-field for Recently Reported Nb_3Sn based CICC Cable.

Design Name	ITER TF option 2	ITER TF option 1	CSIO2 right	TFPRO2 OST1	MF HFML STP	ITER CS STP	TFPRO2 OST2	CSIO2 left	MF HFML LTP	CSIO1 right	CSIO1 left	ITER CS original	PITSAM 5S	PITSAM 2	PITSAM 5L
No. of elements, N_i															
1st stage	2	2	2	2	1 or 2	2	2	2	1 or 2	2	3	2	1 or 2	1 or 2	1 or 2
2nd stage	3	3	3	3	4	3	3	3	4	3	3	3	3	3	3
3rd stage	5	5	4	5	4	4	5	4	4	4	4	4	3	3	3
4th stage	5	5	4	5	5	4	5	4	5	4	4	4	4	4	4
5th stage	6	6	6	6		6	6	6		6	6	6			
Twist Pitch, λ_i (mm)															
1st stage	80	45	110	45	20	20	116	22	82	45	45	45	33	58	83
2nd stage	140	85	115	87.5	45	45	182	45	110	83	83	85	95	95	140
3rd stage	190	125	127	126.5	80	80	245	81	135	141	141	145	139	139	192
4th stage	300	250	140	245	160	150	415	159	160	242	252	250	213	213	213
5th stage	420	450	385	460		450	440	443		423	423	450			
$\prod_{m=0}^{i-1} N_m$															
1st stage	1	1	1	1	1	1	1	1	1	1	1	1	1	1	1
2nd stage	2	2	2	2	1	2	2	2	1	2	3	2	1	1	1
3rd stage	6	6	6	6	6	6	6	6	6	6	9	6	4	4	4
4th stage	30	30	24	30	24	24	30	24	24	24	36	24	12	12	12
5th stage	150	150	96	150		96	150	96		96	144	96			
r_i/λ_i															
1st stage	0.00592	0.01052	0.00431	0.01039	0.02338	0.02367	0.00403	0.02157	0.00570	0.01052	0.01052	0.01065	0.01417	0.00806	0.00563
2nd stage	0.00729	0.01200	0.00889	0.01152	0.02509	0.02267	0.00554	0.02272	0.01026	0.01229	0.01229	0.01215	0.01061	0.01061	0.00720
3rd stage	0.01450	0.02204	0.01944	0.02152	0.03407	0.03078	0.01111	0.03048	0.02019	0.01747	0.01747	0.01719	0.01562	0.01562	0.01131
4th stage	0.02548	0.03058	0.04257	0.03082	0.04602	0.03964	0.01819	0.03748	0.04602	0.02457	0.02359	0.02407	0.02461	0.02461	0.02461
5th stage	0.05460	0.05096	0.04644	0.04924		0.03964	0.05148	0.04036		0.04217	0.04217	0.04012			
$\frac{N_i}{\lambda_i}\frac{2\pi r_i/\lambda_i}{\sqrt{(2\pi r_i/\lambda_i)^2+1}}\prod_{m=0}^{i-1} N_m$ (mm^{-1})															
1st stage	0.00093	0.00293	0.00049	0.00290	0.00727	0.01471	0.00044	0.01221	0.00044	0.00293	0.00440	0.00297	0.00269	0.00087	0.00043
2nd stage	0.00196	0.00531	0.00291	0.00495	0.02076	0.01880	0.00115	0.01885	0.00351	0.00557	0.00835	0.00537	0.00280	0.00280	0.00129
3rd stage	0.01433	0.03293	0.02291	0.03177	0.06280	0.05697	0.00853	0.05573	0.02237	0.01857	0.02785	0.01778	0.00843	0.00843	0.00443
4th stage	0.07904	0.11320	0.17719	0.11639	0.20832	0.15467	0.04105	0.13842	0.20832	0.06052	0.08379	0.05743	0.03444	0.03444	0.03444
5th stage	0.69535	0.60988	0.41909	0.57831		0.30933	0.62953	0.31962		0.34874	0.52311	0.31288			
Sum	0.79161	0.76424	0.62259	0.73433	0.29915	0.55448	0.68069	0.54482	0.23464	0.43633	0.64750	0.39642	0.04836	0.04654	0.04058
$B_{\parallel}$ (T)	0.075	0.073	0.067	0.070	0.063	0.059	0.065	0.058	0.049	0.047	0.046	0.042	0.022	0.021	0.018
$B_{\Phi\,\max}$ (T)	0.593	0.593	0.548	0.600	0.543	0.549	0.600	0.548	0.543	0.549	0.549	0.543	0.649	0.649	0.649
$B_{\parallel}/B_{\Phi\,\max}$	0.127	0.122	0.121	0.116	0.115	0.108	0.108	0.106	0.090	0.085	0.084	0.078	0.033	0.032	0.028

where r_i and λ_i are respectively the radius and twist pitch of the ith stage sub-cable. Values for N_i are given in Table III, and the multiplying factors r_i/r_s where r_s is the radius of a cable strand are calculated in Table II. For r_i, however, there should also be multiplying correction factors k_i that adjust the r_i values for packing. It is assumed here that these factors can be ignored for the calculation of a rough estimate of the zeroth order field. As an indication of the difference with and without k_i, the ratio between the final target cable radius which is 16.3 mm and r_5 with k_i=1 is approximately 0.914 for ITER CS CICC cable.

3.3. Longitudinal Current in Final Cable

For the longitudinal current, the total current in the final cable can be described as $j_s \prod_{m=0}^{5} N_m$ which is simply j_s multiplied by the total number of superconducting strands. A correction factor for the current in the Cu strands should be included but is ignored for simplification. And as mentioned earlier, uniformity of the current over the whole circular cable cross section is also assumed.

3.4. Resulting Internal Self-field of Cable

The final simplified model of the magnetostatic self-field inside ITER CS cable is an azimuthal field B_Φ around the central axis of the cable in combination with a longitudinal field $B_\parallel$ along the length of the cable. The magnitude of B_Φ estimated using Ampère's law with a straight infinite conductor is proportional to the distance from the central axis and has a maximum value of

$$B_{\Phi\,\max} = 576\mu_0 j_s / 2\pi r_5 \tag{6}$$

at the rim. The longitudinal field $B_\parallel$ is uniform inside the cable and has a magnitude given by $\mu_0 j/\Delta z$ also for a straight infinite conductor.

Using the parameter values in Tables I, II and III, B_Φ and $B_\parallel$ can be calculated, and the results are included in Table III. In addition, the individual terms that went into the calculation of $j/\Delta z$ for $B_\parallel$ are also tabulated. It can be seen that the contribution to $B_\parallel$ increases with higher stage terms and that the largest term from the final stage is dominant.

In order to make proper comparisons between different cable designs, the ratio $B_\parallel/B_{\Phi\,\max}$ is used, which allows comparison independent of the total current through the cable. Besides the ITER CS CICC cable, calculations of $B_\parallel/B_{\Phi\,\max}$ have been performed for cable in other Nb_3Sn CICC including the ITER TF conductor and other CICCs tested and reported in the recent past [39-42]. The cable characteristics and calculations for each cable design are given in descending order of $B_\parallel/B_{\Phi\,\max}$ in Tables I and III.

3.5. Discussion on Validity of the Model

Besides the assumptions and simplifications already mentioned in the cable model for the ITER CS CICC, it was also assumed, for analysis described later, that the characteristic length scale for individual strand or sub-cable is short compared to the next stage sub-cable and final cable, *i.e.* $\lambda_i \ll \lambda_{i+1}$. However, this is not fully the case, as the average twist pitch ratio (β_λ) given by

$$\beta_\lambda = \frac{1}{N_{max}-1} \sum_{i=1}^{N_{max}-1} \frac{\lambda_{i+1}}{\lambda_i}, \tag{7}$$

where N_{max} is the number of sub-cable stages in the cable, is only between 1.2 and 2.3 for the CICCs in Table I.

The cable is also assumed to be cylindrical. Other shapes will introduce nonuniformity in the field. However, such nonuniformity seems to result in better T_{cs} performance as seen in square and rectangular CICCs [42, 43]. The analysis of the cable layouts then still provides relevant information for cable comparisons.

On the other hand, there is nonuniformity of field in CICC cable stemming from the current distribution across the face of the cable, which can degrade performance. The Cu strands in the cable have already been determined to have an effect [6, 7, 35]. But, current distribution inside CICC does not seem to be easily controlled and can be affected by external factors making it difficult to predict as well.

In terms of temporal assumptions, the model has been developed to explain the results of the ITER CICC performance tests with pseudo direct current [10]. Though AC performance of the CICC using the cable model could be inferred, such as that ITER CS CICC with STP cable would have larger AC losses than original design cable, comparisons or detailed studies of AC test results have yet to be performed with the model. The results of such studies could be compared with investigations that have already taken place with more sophisticated cable models which predict coupling losses that are dependent on β_λ [24, 44].

Finally, in real ITER TF and CS layout CICCs, there is a central cooling spiral in the middle of the cable as seen in Fig. 1. This cooling channel or hole would predict a larger $B_\parallel$ in the cable. However, this has been ignored for simplicity, and considerations for these factors are left to a more sophisticated study. As such, any conclusions in this paper should only be regarded as indicative.

4. COMMENTS ON THE CALCULATIONS ON CICC CABLE LAYOUTS

4.1. Comparisons between ITER CS CICC Cable Designs

There were six ITER CS layout type CICC cables for which calculations were performed. The resulting calculations for $B_\parallel$ showed an increase of around 60%, going from the smallest to the largest $B_\parallel$. Interestingly, among the CICC cables with ITER CS layout, the largest $B_\parallel$ was in "CSIO2 right" which had the longest λ_1 and λ_2 but the smallest β_λ. The short λ_4 and λ_5 were the cause for the large $B_\parallel/B_{\Phi\,\max}$. Furthermore, despite predictions that as $\beta_\lambda \rightarrow 1$, better performance should be observed, "CSIO2 right" showed degradation in T_{cs} [12, 24].

4.2. Calculations for ITER TF Type Conductor Cable

Unlike in the ITER CS layout, there is a Cu core in the fourth stage sub-cable which complicated the calculation of r_4/r_s in the ITER TF layout. Using the dimensions of the third stage sub-cable, the size of the opening in the middle of a fourth stage sub-cable packed in the form of a pentagon was calculated and was determined to be smaller

than the size of the Cu core, though not by much. So, r_4/r_s was determined using the configuration of a circle of radius r_3, which represents a third stage sub-cable, that touches a circle of radius $\left(1+\sqrt{2}\right)\left(1+2/\sqrt{3}\right)r_s$ which represents a Cu core.

It is also noted that the size of the opening formed in the fifth stage final cable is large enough for a 10 mm diameter cooling spiral to fit inside. Regardless, this did not affect the expression for r_5/r_s due to simplification, as mentioned earlier.

Additionally, in some ITER TF layout CICC samples, the Cu strand had a slightly different diameter than the Nb_3Sn strand. This difference was also ignored for simplicity.

4.3. Calculations on Square and Rectangular CICC Cable

The MF SCH layout and the PITSAM layout had an even more complex complication than the ITER TF layout. Not all first stage sub-cables in the second stage were identical. Specifically, some first stage sub-cable had only one Nb_3Sn strand while others had two.

In order to reflect this in the calculation for $B_\parallel$, the first stage sub-cable was calculated as having only one Nb_3Sn strand, but then during the calculation for the second stage sub-cable, the additional contribution of the remaining Nb_3Sn strands to the second stage sub-cable twist pitch was added. This correction omits the contribution of the additional Nb_3Sn strands to the first stage sub-cable twist pitch. Fortunately, these contributions should be on the order of the contribution of the first stage sub-cable with one Nb_3Sn strand, which are small compared to the total. Thus, the deviation is small and should be acceptable for a rough estimate of $B_\parallel$.

The values of $B_\parallel/B_{\Phi\,\max}$ of the PITSAM layout CICC cables are a factor of 2 or more lower than the cable with the next highest $B_\parallel/B_{\Phi\,\max}$, forming a group of their own. Recalling that square or rectangular CICC cable show better T_{cs} performance than circular cable, the gap in $B_\parallel/B_{\Phi\,\max}$ with other cables may not be that significant [43]. Nevertheless, all PITSAM layout CICCs studied here showed degradation in T_{cs} [39, 42].

5. DISCUSSION OF THE RESULTS

5.1. Trends and Correlation with T_{cs} Performance

The initial rise in T_{cs} with cyclic EM loading seen during testing at SULTAN was only consistently observed with CICCs that used the ITER CS layout with STP cabling. These CICCs correspond to CICC samples "ITER CS STP" and "CSIO2 left" which have values of $B_\parallel/B_{\Phi\,\max}$ around 0.11. Other CICC samples with $B_\parallel/B_{\Phi\,\max} \approx 0.11$ also showed superior performance over other samples. These include "TFPRO2 OST2", "MF HFML STP" and "MF HFML LTP", the latter two being rectangular CICCs.

Whether there is an initial increase in T_{cs} is a little unclear for "MF HFML STP" and "MF HFML LTP", but stability was good up to 2000 EM cycles after which "MF HFML LTP" definitely showed degradation [41]. It may be the case that if circular cables were used, tests would have shown inferior performance, for at least "MF HFML LTP".

In the case of "TFPRO2 OST2", no significant initial T_{cs} increase was observed. However, "TFPRO2 OST2" is also characterized by a comparatively very small void fraction of 27.7%, only higher than "MF HFML STP" and "MF HFML LTP" [40]. The small void fraction may have prevented increases in T_{cs}, while the cabling that resulted in $B_\parallel/B_{\Phi\,\max} \approx 0.11$ may have prevented degradation.

These results suggest that the internal magnetostatic self-field of Nb_3Sn CICC are interacting with the cable in such a way that as $B_\parallel$ increases with respect to B_Φ, T_{cs} performance improves, until after some peak further increases in $B_\parallel$ with respect to B_Φ become detrimental.

5.2. Possible Link with Strand Strain Relaxation

Efforts have been made to link the increase in $B_\parallel$ due to STP cabling with increases in cable strand tension or hoop stress. For the most part, $B_\parallel$ only interacts with the circular transverse current and B_Φ only with the longitudinal current. The direction of the forces on the circular transverse currents is radial, with the circular currents pushing the CICC cable and sub-cables outwards. This can be regarded as the circular transverse currents attempting to restore the thermally contracted radii. From Fig. 2 and the data or information in [6], [20-22], [45] and [46], a cumulative reverse tensile strain (ε) of only 0.05% in the Nb_3Sn strands can explain the total T_{cs} increase in ITER CS CICC samples with STP cable, which is consistent with a finding in [16]. Calculation of the strand stress (σ) were attempted and using the relation

$$\varepsilon = \sigma/E \tag{8}$$

where E is the modulus of elasticity of the Nb_3Sn strands, the strain can be estimated and matched to prediction.

The values of E for ITER relevant Nb_3Sn strand are reported to be on the order of 10^{11} Pa for the axial modulus and on the order of 10^9 Pa for the transverse modulus at 4 K [11, 21-25, 47-52]. Using these values, however, calculations show that direct axial strain in the Nb_3Sn strands from axial stress is too small. Estimates on the relaxation of bending strain also arrive at the same result.

On the other hand, a possible mechanism that could explain the strain relaxation is the behavior of transverse E for small values of σ. It has been observed that for ITER relevant Nb_3Sn strand, the value of transverse E is initially at most on the order of 10^8 Pa for small contact loads [11, 22, 52]. Thus, with radially outward forces acting on the strands, the strands shall initially thin out with expansion in the transverse direction, and the thinning will partly result in additional axial elongation due to the Poisson Effect with a Poisson's ratio of around 0.3 for Nb_3Sn [53]. To make the values consistent, initial inter-strand contact stress on the order of 10^5 Pa is needed, and estimation of this value in ITER CS STP cable is still on going.

As transverse ε increases, transverse E increases dramatically by a factor of 10 or more to 10^9 Pa at around 1%-5% strain. This along with the rigidity of the cable and surrounding boundary inhibits further large increases in ε and consequently, the I_c of the Nb_3Sn strands. It is also the

case that with large transverse ε, the superconducting filaments in the strands will start to fracture leading to I_c and T_{cs} degradation [6, 20, 21, 25-27, 39, 49-52].

5.3. Absence of a Definitive Explanation on T_{cs} Behavior

Considering the effect of B_Φ on CICC cable, the forces on the longitudinal current push the cable strands and sub-cables inwards toward the cable axis. An estimate of the forces involved can be easily calculated given the values of $B_{\Phi\,\max}$ which are between 0.54 T and 0.65 T for the CICCs samples in Table III. It should be noted that these values are larger than the estimates of $B_\parallel$ by about an order of magnitude.

For ITER CS STP cable, the nominal current through the cable is 49 kA. From this, the accumulated inward force per unit length of cable due to B_Φ is calculated to be about 18 kN/m. Furthermore, performance testing on ITER conductor samples at SULTAN is performed with a background field of nearly 11 T. For ITER CS CICC, the cable experiences a transverse force per length of cable greater than 530 kN/m which translates to about 15.8 MPa of pressure. This pressure was strong enough to deform CS cable samples during testing, contributing to T_{cs} degradation in original design CICC [4-6].

The combination of the above considerations suggests that a full and proper explanation of T_{cs} behavior in ITER CS STP CICC must take into consideration other factors besides the internal self-field, such as the cable rigidity. Therefore, a more detailed cable model or modifications of existing cable numerical models will be required to fully explain and predict T_{cs} performance. These models should reproduce the internal self-field and present the mechanism that balances the internal forces of the CICC cable.

6. OTHER IDENTIFIED FACTORS IN CICC PERFORMANCE

The major factors that influence T_{cs} performance in CICC have already been mentioned. Nevertheless, there are other factors that have also been identified as contributing to conductor performance. For example, the role of the CICC jacket and the jacketing process in affecting conductor T_{cs} and in turn, strand I_c has been studied [4-6, 9-11, 13-16, 24-28, 48, 51, 54]. These studies have mostly concentrated on the axial compression of Nb_3Sn cable from the larger thermal contraction of the jacket material compared to the strand. The results of the studies to date, however, are somewhat inconclusive on whether conductor T_{cs} is affected in any significant way.

On the other hand, the CICC jacket does act as a limiting barrier constricting movement of the cable and compressing the cable and strands even during the manufacturing process. This is clear from destructive examination of CICC samples [4-6, 20]. The jacket and central cooling spiral act as the most outer and inner layer barriers and boundary to the cable with compression of the strands from the rigid jacket or cooling spiral having detrimental effects. If too much pressure is applied during cabling or jacket compaction, the superconducting filaments of the strands will become damaged reducing the maximum cable I_c [6, 14, 15, 46].

7. CONCLUSION

In this paper, estimates of the internal magnetostatic self-field are provided for various Nb_3Sn CICCs that were tested and reported on in the recent past, including the ITER TF and CS conductors. Additionally, the simple CICC cable model and the technique used in the estimations are explained. The results suggest that there is interaction between the self-field and cable such that the longitudinal component and the azimuthal component of the fields counter act each other and that there exists an optimal combination of the field components resulting from the choice of cable layout that maximizes or at least stabilizes T_{cs} performance.

ACKNOWLEDGMENT

The author wishes to thank the members of the Superconductivity Technology Team at ITER Korea, the Superconductor Systems & Auxiliaries Section at the ITER International Organisation, the ITER team at the Japan Atomic Energy Agency, the various superconductor testing laboratories working for ITER and the industrial partners that have provided data, information and documents to make this paper possible.

The views and opinions expressed herein do not necessarily reflect those of the National Fusion Research Institute nor the ITER International Organization.

REFERENCES

[1] N. Mitchell, A. Devred, P. Libeyre, B. Lim, F. Savary, and ITER MAGNET DIVISION, "The ITER magnets: design and construction status," *IEEE Trans. Appl. Supercond.*, vol. 22, no. 3, Art. ID. 4200809, 2012.

[2] P. Libeyre, D. Bessette, M. Jewell, C. Jong, C. Lyraud, F. Rodriguez-Mateos, K. Hamada, W. Reiersen, N. Martovetsky, C. Rey, R. Hussung, S. Litherland, K. Freudenberg, L. Myatt, E. Dalder, R. Reed, and S. Sgobba, "Addressing the technical challenges for the construction of the ITER central solenoid," *IEEE Trans. Appl. Supercond.*, vol. 22, no. 3, Art. ID. 4201104, 2012.

[3] D. Everitt, W. Reiersen, N. Martovetsky, R. Hussung, S. Litherland, K. Freudenberg, L. Myattl, D. Hatfield, M. Cole, D. K. Irick, R. Reed, C. Lyraud, P. Libeyre, D. Bessette, C. Jong, N. Mitchell, F. Rodriguez-Mateos, and N. Dolgetta, "ITER central solenoid design," presented at the 25th Symp. Fusion Eng., San Francisco, June 2013.

[4] Y. Nabara, T. Hemmi, H. Kajitani, H. Ozeki, M. Iguchi, Y. Nunoya, T. Isono, Y. Takahashi, K. Matsui, N. Koizumi, M. Oshikiri, Y. Uno, F. Tsutsumi, H. Nakajima, K. Okuno, K. Sedlak, B. Stepanov, and P. Bruzzone, "Examination of Nb_3Sn conductors for ITER central solenoids," *IEEE Trans. Appl. Supercond.*, vol. 23, no. 3, Art. ID. 4801604, 2013.

[5] T. Hemmi, Y. Nunoya, Y. Nabara, M. Yoshikawa, K. Matsui, H. Kajitani, K. Hamada, T. Isono, Y. Takahashi, N. Koizumi, H. Nakajima, B. Stepanov, and P. Bruzzone, "Test results and investigation of Tcs degradation in Japanese ITER CS conductor samples," *IEEE Trans. Appl. Supercond.*, vol. 22, no. 3, Art. ID. 4803305, 2012.

[6] A. Devred, I. Backbier, D. Bessette, G. Bevillard, M. Gardner, C. Jong, F. Lillaz, N. Mitchell, G. Romano, and A. Vostner, "Challenges and status of ITER conductor production," *Supercond. Sci. Technol.*, vol. 27, no. 4, Art. ID. 044001, 2014.

[7] A. Devred, D. Bessette, P. Bruzzone, K. Hamada, T. Isono, N. Martovetsky, N. Mitchell, Y. Nunoya, K. Okuno, I. Pong, W. Reiersen, C. M. Rey, B. Stepanov, Y. Takahashi, and A. Vostner, "Status of conductor qualification for the ITER central solenoid," *IEEE Trans. Appl. Supercond.*, vol. 23, no. 3, Art. ID. 6001208, 2013.

[8] P. Bruzzone, A. Anghel, A. Fuchs, G. Pasztor, B. Stepanov, M. Vogel, and G. Vecsey, "Upgrade of operating range for SULTAN test facility," *IEEE Trans. Appl. Supercond.*, vol. 12, no. 1, pp. 520-523, 2002.

[9] P. Bruzzone, B. Stepanov, R. Wesche, C. Calzolaio, S. March, and M. Vogel, "Operation and test results from the SULTAN test facility," *IEEE Trans. Appl. Supercond.*, vol. 22, no. 3, Art. ID. 9501704, 2012.

[10] M. Breschi, A. Devred, M. Casali, D. Bessette, M. C. Jewell, N. Mitchell, I. Pong, A. Vostner, P. Bruzzone, B. Stepanov, T. Boutboul, N. Martovetsky, K. Kim, Y. Takahashi, V. Tronza, and W. Yu, "Results of the TF conductor performance qualification samples for the ITER project," *Supercond. Sci. Technol.*, vol. 25, no. 9, Art. ID. 095004, 2012.

[11] A. Nijhuis and Y. Ilyin, "Transverse load optimization in Nb_3Sn CICC design; influence of cabling, void fraction and strand stiffness," *Supercond. Sci. Technol.*, vol. 19, no. 9, pp. 945-962, 2006.

[12] A. Nijhuis, G. Rolando, C. Zhou, E. P. A. van Lanen, J. van Nugteren, R. P. Pompe van Meerdervoort, H. J. G. Krooshoop, W. A. J. Wessel, A. Devred, A. Vostner, and I. Pong, "Optimization of interstrand coupling loss and transverse load degradation in ITER Nb_3Sn CICCs," *IEEE Trans. Appl. Supercond.*, vol. 23, no. 3, Art. ID. 4201206, 2013.

[13] D. Bessette, "Design of a Nb_3Sn cable-in-conduit conductor to withstand the 60 000 electromagnetic cycles of the ITER central solenoid," *IEEE Trans. Appl. Supercond.*, vol. 24, no. 3, Art. ID. 4200505, 2014.

[14] Y. Takahashi, Y. Nabara, H. Ozeki, T. Hemmi, Y. Nunoya, T. Isono, K. Matsui, K. Kawano, M. Oshikiri, Y. Uno, F. Tsutsumi, K. Shibutani, T. Kawasaki, K. Okuno, Y. Murakami, M. Tani, G. Sato, Y. Nakata, and M. Sugimoto, "Cabling technology of Nb_3Sn conductor for ITER central solenoid," *IEEE Trans. Appl. Supercond.*, vol. 24, no. 3, Art. ID. 4802404, 2014.

[15] T. Suwa, Y. Nabara, H. Ozeki, T. Hemmi, T. Isono, Y. Takahashi, K. Kawano, M. Oshikiri, F. Tsutsumi, K. Shibutani, Y. Nunoya, K. Okuno, K.-H. Sim, P.-Y. Park, K. Jang, J.-S. Lee, I.-Y. Han, S. P. Kwon, S.-H. Park, K. Sedlak, B. Stepanov, and P. Bruzzone, "Analysis of internal-tin Nb_3Sn conductors for ITER central solenoid," *IEEE Trans. Appl. Supercond.*, vol. 25, no. 3, Art. ID. 4201704, 2015.

[16] Y. Nabara, T. Hemmi, H. Kajitani, H. Ozeki, T. Suwa, M. Iguchi, Y. Nunoya, T. Isono, K. Matsui, N. Koizumi, F. Tsutsumi, Y. Uno, M. Oshikiri, K. Shibutani, Y. Takahashi, K. Okuno, Y. Murakami, T. Miyatake, M. Sugimoto, A. Takagi, Y. Nakada, K. Miyashita, K. Sedlak, B. Stepanov, and P. Bruzzone, "Impact of cable twist pitch on T_{cs}-degradation and AC loss in Nb_3Sn conductors for ITER central solenoids," *IEEE Trans. Appl. Supercond.*, vol. 24, no. 3, Art. ID. 4200705, 2014.

[17] Change of CS strand and cable parameters, ITER International Organization, St. Paul-lez-Durance, France, PCR-509 UID_ETGT7U, Oct. 2013.

[18] A. Devred, I. Backbier, D. Bessette, G. Bevillard, M. Gardner, M. Jewell, N. Mitchell, I. Pong, and A. Vostner, "Status of ITER conductor development and production," *IEEE Trans. Appl. Supercond*., vol. 22, no. 3, Art. ID. 4804909, 2012.

[19] Technical Specification Annex B to Procurement Arrangement 1.1.P6B.JA.01, ITER International Organization, St. Paul-lez-Durance, France, IDM Doc. ITER_D_2ZQ7Q9 v1.5, Nov. 2009.

[20] C. Sanabria, P. J. Lee, W. Starch, I. Pong, A. Vostner, M. C. Jewell, A. Devred, and D. C. Larbalestier, "Evidence that filament fracture occurs in an ITER toroidal field conductor after cyclic Lorentz force loading in SULTAN," *Supercond. Sci. Technol.*, vol. 25, no. 7, Art. ID. 075007, 2012.

[21] A. Nijhuis, Y. Miyoshi, M. C. Jewell, W. Abbas, and W. A. J. Wessel, "Systematic study on filament fracture distribution in ITER Nb_3Sn strands," *IEEE Trans. Appl. Supercond.*, vol. 19, no. 3, pp. 2628-2632, 2009.

[22] A. Nijhuis, Y. Ilyin, S. Wessel, E. Krooshoop, L. Feng, and Y. Miyoshi, "Summary of ITER TF Nb_3Sn strand testing under axial strain, spatial periodic bending and contact stress," *IEEE Trans. Appl. Supercond.*, vol. 19, no. 3, pp. 1516-1520, 2009.

[23] A. Nijhuis and W. M. de Rapper, "Solution for Lorentz forces response and degradation in Nb_3Sn cable in conduit conductors; verification of cabling effect," *IEEE Trans. Appl. Supercond.*, vol. 18, no. 2, pp. 1491-1495, 2008.

[24] A. Nijhuis, E. P. A. van Lanen, and G. Rolando, "Optimization of ITER Nb_3Sn CICCs for coupling loss, transverse electromagnetic load and axial thermal contraction," *Supercond. Sci. Technol.*, vol. 25, no. 1, Art. ID. 015007, 2012.

[25] A. Nijhuis, Y. Ilyin, W. Abbas, B. ten Haken, and H. H. J. ten Kate, "Performance of an ITER CS1 model coil conductor under transverse cyclic loading up to 40,000 cycles," *IEEE Trans. Appl. Supercond.*, vol. 14, no. 2, pp. 1489-1494, 2004.

[26] N. Mitchell, "Assessment of conductor degradation in the ITER CS insert coil and implications for the ITER conductors," *Supercond. Sci. Technol.*, vol. 20, no. 1, pp. 25-34, 2007.

[27] C. Calzolaio and P. Bruzzone, "Analysis of the CICC performance through the measurement of the thermal strain distribution of the Nb_3Sn filaments in the cable cross section," *IEEE Trans. Appl. Supercond.*, vol. 24, no. 3, Art. ID. 4802204, 2014.

[28] S. P. Kwon, S.-H. Park, W. Park, H. Choi, Y. J. Ma, Y.-H. Seo, B. Stepanov, and P. Bruzzone, "Manufacturing and preliminary performance expectations of Nb_3Sn based conductors allocated for the first ITER TF coil with CICC from Korea," *IEEE Trans. Appl. Supercond.*, vol. 24, no. 3, Art. ID. 4801605, 2014.

[29] I.-Y. Han, Nexans Korea, Cheongju, Chungcheongbuk-do, 28183, Republic of Korea, personal communication, 2013.

[30] G. Pasztor, P. Bruzzone, A. Anghel, and B. Stepanov, "An alternative CICC design aimed at understanding critical performance issues in Nb_3Sn conductors for ITER," *IEEE Trans. Appl. Supercond.*, vol. 14, no. 2, pp. 1527-1530, 2004.

[31] J. R. Moser and R. F. Spencer, Jr., "Predicting the magnetic fields from a twisted-pair cable," *IEEE Trans. Electromagn. Compat.*, vol. EMC-10, no. 3, pp. 324-329, 1968.

[32] Y. J. Chen and J. P. Freidberg, "A method for modeling the winding pattern of a large scale superconducting cable," *IEEE Trans. Magn.*, vol. 32, no. 5, pp. 5145-5147, 1996.

[33] J. Feng, "A cable twisting model and its application in CSIC multi-stage cabling structure," *Fusion Eng. Design*, vol. 84, no. 12, pp. 2084–2092, 2009.

[34] A. S. Nemov, D. P. Boso, I. B. Voynov, A. I. Borovkov, and B. A. Schrefler, "Generalized stiffness coefficients for ITER superconducting cables, direct FE modeling and initial configuration," *Cryogenics*, vol. 50, no. 5, pp. 304-313, 2010.

[35] J. Qin, L. L. Warnet, Y. Wu, and A. Nijhuis, "CORD, a novel numerical mechanical model for Nb_3Sn CICCs," *IEEE Trans. Appl. Supercond.*, vol. 21, no. 3, pp. 2046-2049, 2011.

[36] E. P. A. van Lanen, A. Nijhuis, "JackPot: a novel model to study the influence of current non-uniformity and cabling patterns in cable-in-conduit conductors," *Cryogenics*, vol. 50, no. 3, pp. 139-148, 2010.

[37] M. Breschi, P. L. Ribani, H. Bajas, and A. Devred, "Modeling of the electro-mechanical behavior of ITER Nb_3Sn cable in conduit conductors," *Supercond. Sci. Technol*., vol. 25, no. 5, Art. ID. 054005, 2012.

[38] S. P. Kwon, "A simplified model of the superconducting cable of the ITER central solenoid conductor under DC bias conditions," presented at the 24th Magnet Technology Conf., Seoul, Rep. of Korea, 2015.

[39] L. Muzzi, G. De Marzi, A. Di Zenobio, and A. della Corte, "Cable-in-conduit conductors: lessons from the recent past for future developments with low and high temperature superconductors," *Supercond. Sci. Technol.*, vol. 28, no. 5, Art. ID. 053001, 2015.

[40] P. Bruzzone, M. Bagnasco, M. Calvi, F. Cau, D. Ciazynski, A. della Corte, A. Di Zenobio, L. Muzzi, A. Nijhuis, E. Salpietro, L. Savoldi Richard, S. Turtù, A. Vostner, R. Wesche, and R. Zanino, "Test results of two European ITER TF conductor samples in SULTAN," *IEEE Trans. Appl. Supercond.*, vol. 18, no. 2, pp. 1088-1091, 2008.

[41] K. Sedlak, P. Bruzzone, B. Stepanov, A. den Ouden, J. Perenboom, A. della Corte, L. Muzzi, A. Di Zenobio, and F. Quagliata, "Test of the MF-CICC conductor designed for the 12-T outsert coil of the

HFML 45-T hybrid magnet," *IEEE Trans. Appl. Supercond.*, vol. 26, no. 4, Art. ID. 4300305, 2016.

[42] P. Bruzzone, B. Stepanov, R. Wesche, A. della Corte, L. Affinito, M. Napolitano, and A. Vostner, "Test results of a Nb_3Sn cable-in-conduit conductor with variable pitch sequence," *IEEE Trans. Appl. Supercond.*, vol. 19, no. 3, pp. 1448-1451, 2009.

[43] A. della Corte, V. Corato, A. Di Zenobio, C. Fiamozzi Zignani, L Muzzi, G. M. Polli, L. Reccia, S. Turt`u, P. Bruzzone, E. Salpietro, and A. Vostner, "Successful performances of the EU-AltTF sample, a large size Nb_3Sn cable-in-conduit conductor with rectangular geometry," *Supercond. Sci. Technol.*, vol. 23, no. 4, Art. ID. 045028, 2010.

[44] G. Rolando, A. Devred, and A. Nijhuis, "Minimizing coupling loss by selection of twist pitch lengths in multi-stage cable-in-conduit conductors," *Supercond. Sci. Technol.*, vol. 27, no. 1, Art. ID. 015006, 2014.

[45] S. Oh, S.-H. Park, C. Lee, Y. Chang, K. Kim, and P.-Y. Park, "Strain dependence of critical current in internal tin process Nb_3Sn strands," *IEEE Trans. Appl. Supercond.*, vol. 15, no. 2, pp. 3462-3465, 2005.

[46] S. P. Kwon, K.-H. Sim, Y. J. Ma, S.-H. Park, P.-Y. Park, I.-S. Shin, H. Choi, Y.-H. Seo, K.-H. Jang, and W. Park, "Prototype Nb_3Sn superconducting strand for ITER CS coil conductor produced in Korea using the internal-tin route," *IEEE Trans. Appl. Supercond.*, vol. 25, no. 3, Art. ID. 4201106, 2015.

[47] N. C. van den Eijnden, A. Nijhuis, Y. Ilyin, W. A. J. Wessel, and H. H. J. ten Kate, "Axial tensile stress-strain characterization of ITER model coil type Nb_3Sn strands in TARSIS," *Supercond. Sci. Technol.*, vol. 18, no. 11, pp. 1523-1532, 2005.

[48] N. Mitchell, "Modeling of the effect of Nb_3Sn strand composition on thermal strains and superconducting performance," *IEEE Trans. Appl. Supercond.*, vol. 15, no. 2, pp. 3572-3576, 2005.

[49] N. Mitchell, "Analysis of the effect of Nb_3Sn strand bending on CICC superconductor performance," *Cryogenics*, vol. 42, no. 5, pp. 311-325, 2002.

[50] N. Mitchell, "Mechanical and magnetic load effects in Nb_3Sn cable-in-conduit conductors," *Cryogenics*, vol. 43, no. 3-5, pp. 255-270, 2003.

[51] N. Mitchell, "Finite element simulations of elasto-plastic processes in Nb_3Sn strands," *Cryogenics*, vol. 45, no. 7, pp. 501-515, 2005.

[52] A. Nijhuis, Y. Ilyin, and W. A. J. Wessel, "Spatial periodic contact stress and critical current of a Nb_3Sn strand measured in TARSIS," *Supercond. Sci. Technol.*, vol. 19, no. 11, pp. 1089-1096, 2006.

[53] M. Sundareswari, S. Ramasubramanian, and M. Rajagopalan, "Elastic and thermodynamical properties of A15 Nb_3X (X = Al, Ga, In, Sn and Sb) compounds – First principles DFT study," *Solid State Commun.*, vol. 150, no. 41-42, pp. 2057-2060, 2010.

[54] P. Bruzzone, R. Wesche, and F. Cau, "Results of thermal strain and conductor elongation upon heat treatment for Nb_3Sn cable-in-conduit conductors," *IEEE Trans. Appl. Supercond.*, vol. 20, no. 3, pp. 470-473, 2010.